Title

Differentiation between subcentimeter carcinomas and benign lesions using kinetic parameters derived from ultrafast dynamic contrast-enhanced breast MRI.

Journal

European Radiology, 30(2)

Authors

Onishi, Natsuko
Sadinski, Meredith
Gibbs, Peter
et al.

Publication Date

2020-02-01

DOI

10.1007/s00330-019-06392-5

Peer reviewed

Published in final edited form as:

Eur Radiol. 2020 February ; 30(2): 756–766. doi:10.1007/s00330-019-06392-5.

Differentiation between Subcentimeter Carcinomas and Benign Lesions Using Kinetic Parameters Derived from Ultrafast Dynamic Contrast-Enhanced Breast MRI

Natsuko Onishi, MD, PhD[1], **Meredith Sadinski, PhD**[1], **Peter Gibbs, PhD**[1,2], **Katherine M. Gallagher, MD**[1], **Mary C. Hughes, MD**[1], **Eun Sook Ko, MD**[1], **Brittany Z. Dashevsky, MD, DPhil**[1,3], **Dattesh D. Shanbhag, PhD**[4], **Maggie M. Fung, M.Eng**[5], **Theodore M. Hunt**[1], **Danny F. Martinez, MS**[1], **Amita Shukla-Dave, PhD**[1,2], **Elizabeth A. Morris, MD**[1], **Elizabeth J. Sutton, MD**[1]

[1]Breast Imaging Service, Department of Radiology, Memorial Sloan Kettering Cancer Center, New York, NY, USA

[2]Department of Medical Physics, Memorial Sloan Kettering Cancer Center, New York, NY, USA

[3]Department of Radiology & Biomedical Imaging, University of California, San Francisco, CA, USA

[4]GE Healthcare, Bangalore, India

[5]GE Healthcare, New York, NY, USA

Abstract

Corresponding Author: Elizabeth J. Sutton suttone@mskcc.org, TEL: 646-888-5455, FAX: 646-888-4912.

Guarantor:
The scientific guarantor of this publication is Elizabeth Sutton.

Conflict of Interest:
Dattesh Shanbhag and Maggie Fung both have employment and stock option (GE Healthcare). The rest of the authors of this manuscript declare no relationships with any companies, whose products or services may be related to the subject matter of the article.

Statistics and Biometry:
One of the authors has significant statistical expertise.

Informed Consent:
Written informed consent was waived by the Institutional Review Board.

Ethical Approval:
Institutional Review Board approval was obtained.

Methodology

- retrospective
- diagnostic study
- performed at one institution

Objectives—To evaluate ultrafast DCE-MRI derived kinetic parameters that reflect contrast agent inflow effects in differentiating between subcentimeter BI-RADS 4–5 breast carcinomas and benign lesions.

Methods—We retrospectively reviewed consecutive 3T-MRI performed from February–October 2017, during which ultrafast DCE-MRI was performed as part of a hybrid clinical protocol with conventional DCE-MRI. In total, 301 female patients with 369 biopsy-proven breast lesions were included. Ultrafast DCE-MRI was acquired continuously over approximately 60 seconds (temporal resolution, 2.7–7.1 seconds/phase) starting simultaneously with the start of contrast injection. Four ultrafast DCE-MRI derived kinetic parameters (maximum slope [MS], contrast enhancement ratio [CER], bolus arrival time [BAT] and initial area under gadolinium contrast agent concentration [IAUGC]) and one conventional DCE-MRI derived kinetic parameter (signal enhancement ratio [SER]) were calculated for each lesion. Wilcoxon rank sum test or Fisher's exact test were performed to compare kinetic parameters, volume, diameter, age, and BI-RADS morphological descriptors between subcentimeter carcinomas and benign lesions. Univariate/multivariate logistic regression analyses were performed to determine predictive parameters for subcentimeter carcinomas.

Results—In total, 125 lesions (26 carcinomas and 99 benign lesions) were identified as BI-RADS 4–5 subcentimeter lesions. Subcentimeter carcinomas demonstrated significantly larger MS and SER, and shorter BAT than benign lesions (p=0.0117, 0.0046, and 0.0102, respectively). MS, BAT, and age were determined as significantly predictive for subcentimeter carcinoma (p=0.0208, 0.0023, and <0.0001, respectively).

Conclusions—Ultrafast DCE-MRI derived kinetic parameters may be useful in differentiating subcentimeter BI-RADS 4 and 5 carcinomas from benign lesions.

Keywords

Breast; Cancer; Magnetic resonance imaging; Kinetics; Differential Diagnosis

Introduction

Breast MRI is highly sensitive for breast cancer detection; further, with technological advances, invasive carcinomas smaller than 0.5 cm are now detectable [1–4]. The literature indicates that over 50% of invasive carcinomas that are detected on high-risk screening breast MRI are smaller than 1 cm, many of which are node negative [5]. However, it has also been reported that subcentimeter suspicious lesions (BI-RADS 4–5 lesions [6]) are less frequently malignant than larger lesions, as shown in a study of 666 consecutive lesions detected on MRI [2] where the positive predictive value was lower for subcentimeter lesions than for larger lesions (16% vs. 28%, p = 0.0002). Thus, there is room for improvement to avoid unnecessary biopsies. One challenge is the considerable kinetic and morphologic overlap in MRI characteristics between subcentimeter carcinomas and benign lesions [7]. especially in lesions smaller than 0.5 cm [3, 4, 8].

Ultrafast breast DCE-MRI protocols are increasingly available clinically as well as discussed in the literature [9–18]. Ultrafast DCE-MRI is characterized by high temporal resolution (usually 4–8 sec) with high spatial resolution, using various acceleration methods e.g.,

parallel imaging, view sharing, and compressed sensing. Ultrafast DCE-MRI in the very early phase (0–60 sec after contrast injection) enables image acquisition at multiple time points, yielding heuristic kinetic parameters that reflect contrast agent inflow effects (e.g., maximum slope of the contrast enhancement versus time curve [9, 18]). The diagnostic utility of these parameters has been proven by many researchers in recent years [9–18], but little is known regarding subcentimeter breast lesions.

We hypothesized that ultrafast DCE-MRI in the very early phase may provide kinetic information helpful for the stratification of subcentimeter suspicious lesions. Our study aimed to evaluate kinetic parameters derived from ultrafast DCE-MRI in differentiating between subcentimeter BI-RADS 4 and 5 carcinomas and benign lesions.

Materials and Methods

Patients and Lesions

The institutional review board approved this single-institution, retrospective Health Insurance Portability and Accountability Act-compliant study and waived the need for informed consent.

From February–October 2017, all breast 3T MRI at our institution included ultrafast DCE-MRI as part of a hybrid DCE-MRI protocol in conjunction with conventional DCE-MRI. Clinical assessments of BI-RADS categorization were judged using only the conventional protocol. Among 1747 consecutive breast 3T MRI including both screening and diagnostic examinations, we identified 499 BI-RADS 4–6 examinations for inclusion (Figure 1). We excluded examinations if no ultrafast DCE-MRI was performed (n = 13), no breast lesion was identified (only lesions in lymph node, skin or reconstructed tissue; n = 16), and if the examination was performed to evaluate treatment response at post-chemotherapy (n = 128). Additionally, we excluded lesions pathologically diagnosed as a special type malignancy (n = 6: malignant lymphoma, 1; malignant phyllodes tumor, 1; invasive metaplastic carcinoma, 2; spindle cell sarcoma, 1; angiosarcoma, 1), lesions with no/minimal residual enhancement after biopsy or surgery (n = 33; invasive carcinoma, 22; ductal carcinomas in situ [DCIS], 11), and lesions without one-to-one pathological diagnosis (n = 59). In total, 298 patients with 368 breast lesions pathologically proven under MRI, ultrasonography, or stereotactic-guided biopsy were eligible. Finally, lesions which were determined to be unsuitable for parameter estimation were excluded during image evaluation.

Lesion volume was used to identify subcentimeter lesions for every lesion type (mass, non-mass enhancement [NME], focus). The group of lesions recommended for biopsy on MRI (BI-RADS 4–5) with a volume of less than 0.523 cm^3 (corresponding to a sphere with a diameter of 1 cm) were referred to as the “Subcentimeter C4&5 Group.” All biopsy-proven lesions depicted on BI-RADS 4–6 examination, regardless of size, were referred to as the “Reference Group.”

MRI

All patients underwent MRI examinations on a 3.0T MRI system (Discovery 750, GE Medical Systems) with a dedicated 16- or 8-channel breast coil in the prone position.

Ultrafast DCE-MR images were acquired using a 3D dual-echo fat-water separated T1-weighted differential sub-sampling with cartesian ordering (DISCO) sequence [19] composed of a full k-space sampling phase followed by 15 (16-channel coil) or 10 phases (8-channel coil) acquired continuously. Conventional DCE-MR images were acquired using a 3D fat-suppressed T1-weighted volume imaging breast assessment (VIBRANT) sequence composed of one pre-contrast and three post-contrast phases labeled as Pre-CE, Post-CE1, Post-CE2 and Post-CE3 (Figure 2). The gadolinium-based contrast agent was administered at a concentration of 0.1 mmol gadobutrol per kg body weight (Gadavist; Bayer Healthcare Pharmaceuticals Inc.) and a rate of 2 ml/sec, followed by 40 ml of saline flush at the same rate.

First, Pre-CE images were acquired for conventional DCE-MRI. Second, after full k-space sampling, 15 or 10 phases of ultrafast DCE-MRI was acquired continuously for approximately 60 sec starting simultaneously with the start of contrast injection. Immediately following ultrafast DCE-MRI, conventional DCE-MRI was acquired continuously at three timepoints. The acquisition parameters were as follows: For ultrafast DCE-MRI using DISCO (using either a 16-and 8-channel coil), TR/TE = 3.8/1.7 msec, flip angle = 10°, field of view = 34 cm, acquired matrix = 212×212, in-plane spatial resolution = 1.6×1.6 mm, thickness = 1.6 mm, temporal resolution = 2.7–7.1 sec, axial orientation. For conventional DCE-MRI using VIBRANT, TR/TE = 7.9/4.3, flip angle = 12°, field of view = 34 cm, acquired matrix = 300×300, in-plane spatial resolution = 1.1×1.1 mm, thickness = 1.1 mm, temporal resolution = ~120 sec, axial orientation.

Kinetic Information and Lesion Size

Using GenIQ (GE Healthcare), kinetic parameters, lesion volume (cm^3), and maximum diameter (cm) were calculated for each lesion based on segmentation performed by one of three radiologists (NO, MCH, and EJS with 7, 10, and 6 years of experience in breast MRI, respectively), who had shown good to excellent inter-reader reliability in a separate preliminary analysis (intraclass correlation coefficient ≥ 0.83). The radiologists had access to radiology reports including clinical information, findings, and BI-RADS category but not to pathological reports. Semi-automatic 3D segmentation (drawing an ROI on each slice to cover the whole lesion) was performed on Post-CE1 and cloned the segmentation to all other phases. The 3D segmentation approach was used rather than the hot spot ROI approach (i.e., placing an ROI on the most suspicious part such as the wash-out part) to avoid potential bias for kinetic parameters. Biopsy markers, artefacts, and necrotic areas, if present, were carefully excluded from the segmentation. The time-signal intensity curves of the segmented volumes and ultrafast DCE-MR images were examined by a single radiologist (NO) and a localized, rigid motion correction technique was applied if patient motion during scanning was apparent. The detailed information of each parameter is as follows:

-Conventional DCE-MRI derived parameter: Signal enhancement ratio (SER) was evaluated as a measure of the delayed phase kinetic assessment in BI-RADS [4, 14, 20, 21].

- SER = 100*(signal of Post-CE1 – signal of Pre-CE) / (average signal of Post-CE2 and Post-CE3 – signal of Pre-CE)

-Ultrafast DCE-MRI derived parameters: Maximum slope (MS) [9, 18], contrast enhancement ratio (CER) [14, 21], bolus arrival time (BAT), and initial area under the gadolinium contrast agent concentration time curve (IAUGC) were evaluated. “Time to enhancement” (BAT relative to the time point where the aorta starts to enhance), is a previously reported parameter indicating the time elapsed between the start of enhancement of the aorta and that of a lesion [11, 18]. BAT was evaluated with the assumption that we may ignore differences in cardiac function and circulation time in patients.

- MS (mMol/sec) = the slope of the steepest part of the concentration curve
- CER = (peak signal – baseline signal) / (baseline signal)
- BAT (sec) = the time from the start of contrast injection to tracer bolus arrival at a lesion
- IAUGC = (area under the tissue concentration curve from BAT to 60 sec from the start of contrast injection) / (area under the arterial input function concentration curve from BAT to 60 sec from the start of contrast injection)

In GenIQ, the first three time points of ultrafast DCE-MRI served as baseline (theoretically pre-contrast) data. Signal intensity was automatically converted to contrast agent concentration.

Morphological Information

Two radiologists (NO and ESK with 7 and 13 years of experience in breast MRI, respectively), blinded to pathological reports, reviewed post-CE1 images for all lesions and evaluated the BI-RADS MRI morphological descriptors in consensus: lesion type, mass shape, mass margin, mass internal enhancement, NME distribution, and NME internal enhancement.

Reference Standard

A careful review of pathological reports of both core biopsy specimens and surgical specimens was performed. For lesions that were diagnosed as a high-risk benign lesion, DCIS, or microinvasive carcinoma on the core biopsy specimen but that were upgraded on the corresponding site of the surgical specimen, the latter diagnosis was used. The reference standard was a binary indicator of whether or not carcinoma was identified on one-to-one pathology. Both invasive carcinoma and DCIS were categorized as “carcinoma.” Normal breast tissues and various type of benign lesions were categorized as “benign lesion.”

Statistical Analysis

All analyses were performed using JMP® Version 10.0.2. (SAS Institute Inc.) or R Version 3.5.1 (R Foundation for Statistical Computing). P values <0.05 were considered statistically significant.

Ultrafast DCE-MRI and conventional DCE-MRI derived kinetic parameters, volume, diameter, patient age, and the BI-RADS morphological descriptors were compared between carcinomas and benign lesions within each group using the Wilcoxon rank sum test or the Fisher’s exact test. For the Subcentimeter C4&5 Group, power analysis for the Wilcoxon

rank sum test was conducted in G*Power Version 3.1.9.3 [22] to determine the sufficient sample size, using $\alpha = 0.05$, power = 0.90, allocation ratio (carcinomas/benign lesions) = 0.25, and effect size d of each ultrafast DCE-MRI derived parameter (calculated from our preliminary data in lesions > 1 cm). Based on these assumptions, the desired sample size was determined to be 100 subcentimeter lesions (carcinomas, 20; benign lesions, 80). Lesion volumes between the Subcentimeter C4&5 Group and the Reference Group were compared using Wilcoxon rank sum test.

Within the Subcentimeter C4&5 Group, multivariate logistic regression analyses were used to determine the predictive parameters for subcentimeter carcinomas. The variables included in the multivariate analysis were selected based on the results of the Wilcoxon rank sum test, Fisher's exact test, and univariate logistic regression analysis. Area under the ROC curve (AUC) was used to evaluate the diagnostic performance of the multivariate logistic regression model and Youden index was used to determine the optimal cut-off point of the model. For the purpose of comparison, AUC of the logistic regression model not including age and age alone were generated. DeLong's test was used to compare the AUCs [23].

Results

Patients and Lesions

Of the 298 patients with 368 lesions evaluated, 2 (0.5%) benign lesions with no enhancement during ultrafast DCE-MRI (i.e., showing enhancement at 60 sec or later after contrast injection) and 27 (7%) lesions (23 lesions < 1 cm, 4 lesions ≥ 1 cm) with severe patient motion during MRI scanning which could not be resolved by motion correction were excluded. In total, 271 patients with 339 lesions were analyzed (Figure 1): 125 patients with 156 lesions (46%) scanned using a 16-channel coil and 146 patients with 183 lesions (54%) scanned using 8-channel coil. The median interval between breast MRI and core biopsy was 8 days (interquartile range [IQR], 6–12) in the Subcentimeter C4&5 Group and 13 days (IQR, 7–21) in the Reference Group. Table 1 shows detailed patient and lesion characteristics.

The Subcentimeter C4&5 Group comprised 125 (37%) of the total 339 lesions, consisting of 26 carcinomas (19 invasive carcinomas, 1 microinvasive carcinoma, and 6 DCIS) (21%) and 99 benign lesions (79%). Of the six DCIS, one lesion was primarily diagnosed as atypical ductal hyperplasia on core biopsy specimen and upgraded to DCIS on surgical specimen. Eleven (11%) of 99 benign lesions were high-risk benign lesions i.e., atypical ductal hyperplasia, atypical lobular hyperplasia, and lobular carcinoma in situ. MRI data were acquired using a 16-channel coil for 59 lesions (47%) and an 8-channel coil for 66 lesions (53%).

The Reference Group comprised 339 lesions consisting of 225 carcinomas (195 invasive carcinomas, 7 microinvasive carcinomas, and 23 DCIS) (66%) and 114 benign lesions (34%). Of the seven microinvasive carcinomas, three lesions were primarily diagnosed as DCIS on core biopsy specimen and upgraded to microinvasive carcinomas on surgical specimen. Of the 23 DCIS, one lesion was primarily diagnosed as atypical ductal hyperplasia on core biopsy specimen and upgraded to DCIS on surgical specimen. High-risk

benign lesions were identified in 13 (11%) of 114 benign lesions. MRI data were acquired using a 16-channel coil for 156 lesions (46%) and an 8-channel coil for 183 lesions (54%).

Kinetic Parameters, Lesion Size, and Age

Ultrafast DCE-MRI and conventional DCE-MRI derived kinetic parameters, volume, diameter, and patient age were compared between carcinomas and benign lesions within each group (Table 2). In the Subcentimeter C4&5 Group, MS, BAT, SER, and age were significantly different between carcinomas and benign lesions ($p = 0.0117$, 0.0102, 0.0046, and 0.0002, respectively). In the Reference Group, all variables (MS, CER, BAT, IAUGC, SER, volume, diameter, and age) were significantly different between carcinomas and benign lesions (MS, CER, BAT, IAUGC, SER, volume, and diameter, $p < 0.0001$; age, $p = 0.0031$). Figures 3 and 4 show representative subcentimeter lesions. Lesion volumes were significantly smaller in the Subcentimeter C4&5 Group (median, 0.113 cm^3; IQR, 0.070–0.233) than in the Reference Group (median, 0.617 cm^3; IQR, 0.161–3.320) ($p < 0.0001$).

Morphological Information

BI-RADS morphological descriptors were compared between carcinomas and benign lesions within each group (Table 3). In the Subcentimeter C4&5 Group, no descriptor presented a significant difference between carcinomas and benign lesions. In the Reference Group, lesion type, mass shape, mass margin, NME distribution, and NME internal enhancement were significantly different between carcinomas and benign lesions (lesion type, mass shape, and mass margin, $p < 0.0001$; NME distribution, $p = 0.0007$; NME internal enhancement, $p = 0.0052$).

Multivariate Logistic Regression Analysis of Subcentimeter BI-RADS 4 and 5 Lesions

For multivariate logistic regression analysis in Subcentimeter C4&5 Group, MS, BAT, SER, and age were considered as candidate predictors. Of these four variables, SER was excluded ($p > 0.05$ on univariate logistic regression analysis). All three variables (MS, BAT, and age) were independently associated with subcentimeter carcinoma in multivariate logistic regression analysis ($p = 0.0208$, 0.0023, and < 0.0001, respectively) (Table 4). ROC curves of the MS + BAT + age model, MS + BAT model, and age alone model demonstrated AUCs of 0.846, 0.704, and 0.738 respectively (Figure 5). The MS + BAT + age model showed significantly higher AUC than the MS + BAT model and the age alone model ($p = 0.01$ and 0.03, respectively). Maximum Youden index of the MS + BAT + age model was shown at the cut-off point of 23% probability for subcentimeter carcinomas with sensitivity, specificity, PPV, and NPV of 81%, 80%, 51%, and 94%, respectively (Table 5). The five false negative lesions at the cut-off point of 23% were: one invasive ductal carcinoma (Luminal type), one invasive lobular carcinoma (Luminal type), one microinvasive carcinoma, and two DCIS.

Discussion

Ultrafast DCE-MRI has the potential to change how breast MRI is performed. Conventional DCE-MRI has been the clinical standard over the past decades because of the need to balance the competing demands between spatial and temporal resolutions [6, 24]. In the

present study, we successfully captured the inflow of contrast agent in subcentimeter lesions at multiple time points using ultrafast DCE-MRI with more than 15 times higher temporal resolution than conventional DCE-MRI. Although the diagnosis of suspicious lesions on breast MRI has been based on morphological and kinetic information on conventional DCE-MRI, it may be the time to incorporate ultrafast DCE-MRI information in breast cancer detection and characterization.

In our study, subcentimeter BI-RADS 4–5 carcinomas demonstrated significantly larger MS and shorter BAT than benign lesions. When all biopsy-proven lesions were included, carcinomas demonstrated significantly larger MS, CER, IAUGC, and shorter BAT than benign lesions. These results show that it may be important to consider lesion size in any discussion of the utility of ultrafast DCE-MRI derived kinetic parameters.

The multivariate logistic regression model using MS, BAT, and age demonstrated high diagnostic performance in differentiating subcentimeter carcinomas from benign lesions, which could potentially lead to a decrease in unnecessary biopsy recommendations. The AUC of this model was higher than that of the model that did not include age, showing that the utility of ultrafast DCE derived parameters is enhanced when combined with patient age. Additionally, it is noteworthy that the majority of the false negative lesions (i.e., lesions at the cut-off point of 23% probability for subcentimeter carcinoma) comprised relatively less aggressive carcinomas (i.e., DCIS, microinvasive carcinoma, and invasive lobular carcinoma) known to present slower increase of enhancement than typical invasive carcinomas in conventional DCE-MRI [25–27]. Further studies with larger cohorts at multiple institutions would be needed to validate the diagnostic performance of ultrafast DCE-MRI.

None of the BI-RADS morphological descriptors on conventional DCE-MRI were significantly different between subcentimeter BI-RADS 4–5 carcinomas and benign lesions. This is consistent with previous reports regarding small breast lesions [4, 7], which demonstrates one possible factor making the differential diagnosis of small lesions difficult in conventional DCE-MRI. Our study shows that adding ultrafast DCE-MRI to conventional DCE-MRI may resolve this issue.

Furthermore, our data begs the question, “Do we need delayed phase kinetic information?” SER is a conventional DCE-MRI derived parameter that indicates the delayed phase kinetic assessment in BI-RADS: persistent, SER <91; plateau, 91 ≤ SER ≤ 111; and washout, 111 < SER [4, 14, 20, 21], SER was significantly different between carcinomas and benign lesions in both the Subcentimeter C4&5 Group and the Reference Group. In the univariate logistic regression analysis, however, SER was not significantly predictive of subcentimeter carcinoma, as opposed to MS and BAT. In previous studies, MS and “time to enhancement” (BAT relative to the time point where the aorta starts to enhance) demonstrated higher accuracy than BI-RADS kinetic analysis in the differentiation between malignant and benign lesions [9, 11]. Another study proved that the utility of ultrafast DCE MRI-derived parameters based on enhancement rate and area under the kinetic curve was comparable to SER [14]. Considering these results, capturing delayed enhancement may not be essential

for diagnosing breast cancer. Further studies would be needed to validate whether and how we should incorporate ultrafast DCE-MRI into current standard protocol.

The concentration curve of our ultrafast DCE-MRI protocol likely reflects early leakage of contrast agent from the vessels into the extravascular extracellular space rather than a pure perfusion effect [9, 28, 29]. Thus, larger MS for carcinoma is congruent with the known pathophysiology of carcinoma with abnormally leaky vasculature [30]. In addition, shorter BAT for carcinomas might reflect tumor vasculature with shunt formation and a low-resistance and high-flow pathway [16, 31, 32].

This study has limitations. First, it was a retrospective study. Second, we included all pathologically proven lesions and the patient population was not controlled, i.e., pre-treatment evaluation, diagnostic purpose, follow-up for BI-RADS 3 lesions, and high-risk screening. Third, subcentimeter lesions were defined as lesions with a volume < 0.523 cm^3, although they are usually defined as those with a maximum diameter < 1 cm in clinical practice. As the emphasis in this study was to evaluate quantitative kinetic information for a whole volume, we used volume rather than maximum diameter to standardize size measurement for every lesion type. Fourth, temporal resolution varied according to the breast coil and breast size. Uniform temporal resolution might be preferable for a more precise evaluation of ultrafast DCE-MRI parameters. Finally, parameter calculation is subject to error from patient motion during scanning. This problem is particularly pronounced in subcentimeter lesions where a single voxel shift could correspond to a significant volume of the lesion. We addressed this with a motion correction step and excluded lesions from analysis when this did not sufficiently correct for misregistration between phases.

In conclusion, MS and BAT, the ultrafast DCE-MRI derived kinetic parameters, may be useful in differentiating between subcentimeter carcinomas and benign lesions. These parameters could decrease the number of unnecessary biopsy recommendations.

Acknowledgements

We thank GE Healthcare for technical support.

Funding

This work was supported by the NIH/NCI P30 Cancer Center Support Grant (CCSG) (P30 CA008748).

This work was supported in part by a grant from the Susan G. Komen Foundation.

This work was supported in part by a grant from the Breast Cancer Research Foundation.

Abbreviations

BAT	bolus arrival time
BI-RADS	Breast Imaging Reporting and Data System
CER	contrast enhancement ratio
DCIS	ductal carcinoma in situ

DISCO	differential sub-sampling with cartesian ordering
IAUGC	initial area under gadolinium contrast agent concentration
MS	maximum slope
NME	non-mass enhancement
SER	signal enhancement ratio
VIBRANT	volume imaging breast assessment

References

1. Abe H, Schmidt RA, Shah RN, et al. (2010) MR-directed ("Second-Look") ultrasound examination for breast lesions detected initially on MRI: MR and sonographic findings. AJR Am J Roentgenol 194:370–377. doi: 10.2214/AJR.09.2707 [PubMed: 20093598]
2. Liberman L, Mason G, Morris EA, Dershaw DD (2006) Does size matter? Positive predictive value of MRI-detected breast lesions as a function of lesion size. AJR Am J Roentgenol 186:426–430. doi: 10.2214/AJR.04.1707 [PubMed: 16423948]
3. Jansen SA, Shimauchi A, Zak L, et al. (2011) The diverse pathology and kinetics of mass, nonmass, and focus enhancement on MR imaging of the breast. J Magn Reson Imaging 33:1382–1389. doi: 10.1002/jmri.22567 [PubMed: 21591007]
4. Raza S, Sekar M, Ong EMW, Birdwell RL (2012) Small masses on breast MR: is biopsy necessary? Acad Radiol 19:412–419. doi: 10.1016/j.acra.2011.12.014 [PubMed: 22277636]
5. Kuhl C, Weigel S, Schrading S, et al. (2010) Prospective multicenter cohort study to refine management recommendations for women at elevated familial risk of breast cancer: the EVA trial. J Clin Oncol 28:1450–1457. doi: 10.1200/JC0.2009.23.0839 [PubMed: 20177029]
6. Morris EA, Comstock CE, Lee CH (2013) ACR BI-RADS® Magnetic Resonance Imaging. ACR BI-RADS® Atlas, Breast Imaging Reporting and Data System
7. Meissnitzer M, Dershaw DD, Feigin K, et al. (2017) MRI appearance of invasive subcentimetre breast carcinoma: benign characteristics are common. Br J Radiol 90:20170102. doi: 10.1259/bjr.20170102 [PubMed: 28452624]
8. Ha R, Sung J, Lee C, et al. (2014) Characteristics and outcome of enhancing foci followed on breast MRI with management implications. Clin Radiol 69:715–720. doi: 10.1016/j.crad.2014.02.007 [PubMed: 24680120]
9. Mann RM, Mus RD, van Zelst J, et al. (2014) A novel approach to contrast-enhanced breast magnetic resonance imaging for screening: high-resolution ultrafast dynamic imaging. Invest Radiol 49:579–585. doi: 10.1097/RLI.0000000000000057 [PubMed: 24691143]
10. Platel B, Mus R, Welte T, et al. (2014) Automated characterization of breast lesions imaged with an ultrafast DCE-MR protocol. IEEE Trans Med Imaging 33:225–232. doi: 10.1109/TMI.2013.2281984 [PubMed: 24058020]
11. Mus RD, Borelli C, Bult P, et al. (2017) Time to enhancement derived from ultrafast breast MRI as a novel parameter to discriminate benign from malignant breast lesions. Eur J Radiol 89:90–96. doi: 10.1016/j.ejrad.2017.01.020 [PubMed: 28267555]
12. Herrmann K-H, Baltzer PA, Dietzel M, et al. (2011) Resolving arterial phase and temporal enhancement characteristics in DCE MRM at high spatial resolution with TWIST acquisition. J Magn Reson Imaging 34:973–982. doi: 10.1002/jmri.22689 [PubMed: 21769981]
13. Pineda FD, Medved M, Wang S, et al. (2016) Ultrafast Bilateral DCE-MRI of the Breast with Conventional Fourier Sampling: Preliminary Evaluation of Semi-quantitative Analysis. Acad Radiol 23:1137–1144. doi: 10.1016/j.acra.2016.04.008 [PubMed: 27283068]
14. Abe H, Mori N, Tsuchiya K, et al. (2016) Kinetic Analysis of Benign and Malignant Breast Lesions With Ultrafast Dynamic Contrast-Enhanced MRI: Comparison With Standard Kinetic

Assessment. AJR Am J Roentgenol 207:1159–1166. doi: 10.2214/AJR.15.15957 [PubMed: 27532897]

15. Heacock L, Gao Y, Heller SL, et al. (2017) Comparison of conventional DCE-MRI and a novel golden-angle radial multicoil compressed sensing method for the evaluation of breast lesion conspicuity. J Magn Reson Imaging 45:1746–1752. doi: 10.1002/jmri.25530 [PubMed: 27859874]
16. Onishi N, Kataoka M, Kanao S, et al. (2018) Ultrafast dynamic contrast-enhanced mri of the breast using compressed sensing: breast cancer diagnosis based on separate visualization of breast arteries and veins. J Magn Reson Imaging 47:97–104. doi: 10.1002/jmri.25747 [PubMed: 28556576]
17. Cheng Z, Wu Z, Shi G, et al. (2018) Discrimination between benign and malignant breast lesions using volumetric quantitative dynamic contrast-enhanced MR imaging. Eur Radiol 28:982–991. doi: 10.1007/s00330-017-5050-2 [PubMed: 28929243]
18. Goto M, Sakai K, Yokota H, et al. (2018) Diagnostic performance of initial enhancement analysis using ultrafast dynamic contrast-enhanced MRI for breast lesions. Eur Radiol 29:1–11. doi: 10.1007/s00330-018-5643-4 [PubMed: 30421017]
19. Saranathan M, Rettmann DW, Hargreaves BA, et al. (2012) Differential Subsampling with Cartesian Ordering (DISCO): a high spatio-temporal resolution Dixon imaging sequence for multiphasic contrast enhanced abdominal imaging. J Magn Reson Imaging 35:1484–1492. doi: 10.1002/jmri.23602 [PubMed: 22334505]
20. Esserman L, Hylton N, George T, Weidner N (1999) Contrast-Enhanced Magnetic Resonance Imaging to Assess Tumor Histopathology and Angiogenesis in Breast Carcinoma. Breast J 5:13–21. [PubMed: 11348250]
21. Shimauchi A, Abe H, Schacht DV, et al. (2015) Evaluation of Kinetic Entropy of Breast Masses Initially Found on MRI using Whole-lesion Curve Distribution Data: Comparison with the Standard Kinetic Analysis. Eur Radiol 25:2470–2478. doi: 10.1007/s00330-015-3635-1 [PubMed: 25698353]
22. Faul F, Erdfelder E, Lang A-G, Buchner A (2007) G*Power 3: a flexible statistical power analysis program for the social, behavioral, and biomedical sciences. Behav Res Methods 39:175–191. doi: 10.3758/BF03193146 [PubMed: 17695343]
23. DeLong ER, DeLong DM, Clarke-Pearson DL (1988) Comparing the areas under two or more correlated receiver operating characteristic curves: a nonparametric approach. Biometrics 44:837–845. doi: 10.2307/2531595 [PubMed: 3203132]
24. Kuhl C (2007) The current status of breast MR imaging. Part I. Choice of technique, image interpretation, diagnostic accuracy, and transfer to clinical practice. Radiology 244:356–378. doi: 10.1148/radiol.2442051620 [PubMed: 17641361]
25. Jansen SA, Newstead GM, Abe H, et al. (2007) Pure ductal carcinoma in situ: kinetic and morphologic MR characteristics compared with mammographic appearance and nuclear grade. Radiology 245:684–691. doi: 10.1148/radiol.2453062061 [PubMed: 18024450]
26. Van Goethem M, Schelfout K, Kersschot E, et al. (2005) Comparison of MRI features of different grades of DCIS and invasive carcinoma of the breast. JBR-BTR 88:225–232. [PubMed: 16302331]
27. Mann RM, Hoogeveen YL, Blickman JG, Boetes C (2008) MRI compared to conventional diagnostic work-up in the detection and evaluation of invasive lobular carcinoma of the breast: a review of existing literature. Breast Cancer Res Treat 107:1–14. doi: 10.1007/s10549-007-9528-5 [PubMed: 18043894]
28. Taylor JS, Reddick WE (2000) Evolution from empirical dynamic contrast-enhanced magnetic resonance imaging to pharmacokinetic MRI. Adv Drug Deliv Rev 41:91–110. [PubMed: 10699307]
29. Cuenod CA, Balvay D (2013) Perfusion and vascular permeability: basic concepts and measurement in DCE-CT and DCE-MRI. Diagn Interv Imaging 94:1187–1204. doi: 10.1016/jdiii.2013.10.010 [PubMed: 24211260]
30. Jain RK (2013) Normalizing tumor microenvironment to treat cancer: bench to bedside to biomarkers. J Clin Oncol 31:2205–2218. doi: 10.1200/JC0.2012.46.3653 [PubMed: 23669226]

31. Pries AR, Hopfner M, le Noble F, et al. (2010) The shunt problem: control of functional shunting in normal and tumour vasculature. Nat Rev Cancer 10:587–593. doi: 10.1038/nrc2895 [PubMed: 20631803]

32. Jain RK, Martin JD, Stylianopoulos T (2014) The role of mechanical forces in tumor growth and therapy. Annu Rev Biomed Eng 16:321–346. doi: 10.1146/annurev-bioeng-071813-105259 [PubMed: 25014786]

Key Points

- Ultrafast DCE MRI can generate kinetic parameters, effectively differentiating breast carcinomas from benign lesions.
- Subcentimeter carcinomas demonstrated significantly larger maximum slope and shorter bolus arrival time than benign lesions.
- Maximum slope and bolus arrival time contribute to better management of suspicious subcentimeter breast lesions.

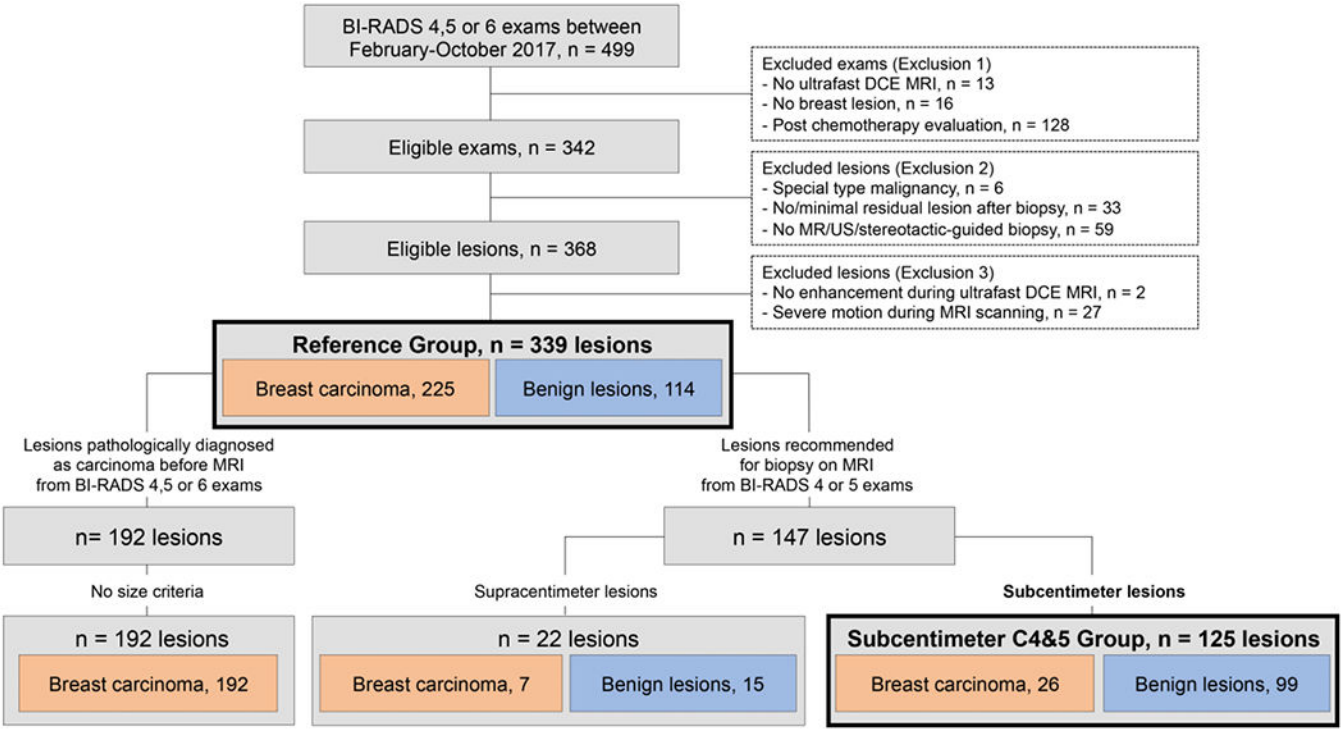

Figure 1:
Flowchart of lesions.

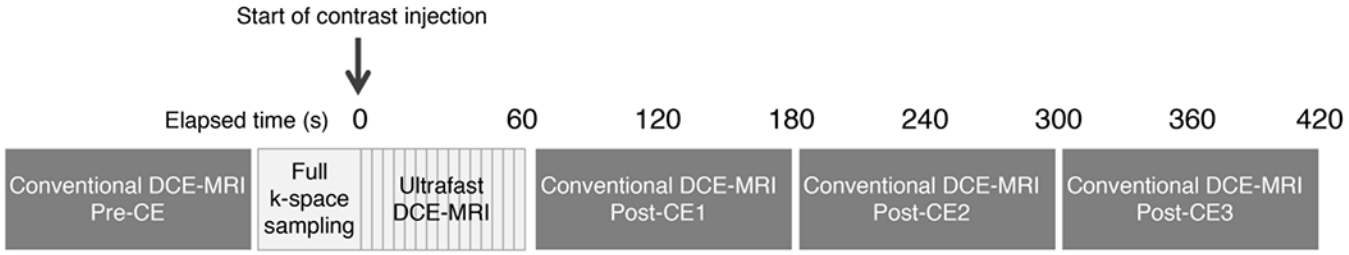

Figure 2:
Hybrid protocol of ultrafast and conventional dynamic contrast-enhanced magnetic resonance imaging (DCE-MRI)

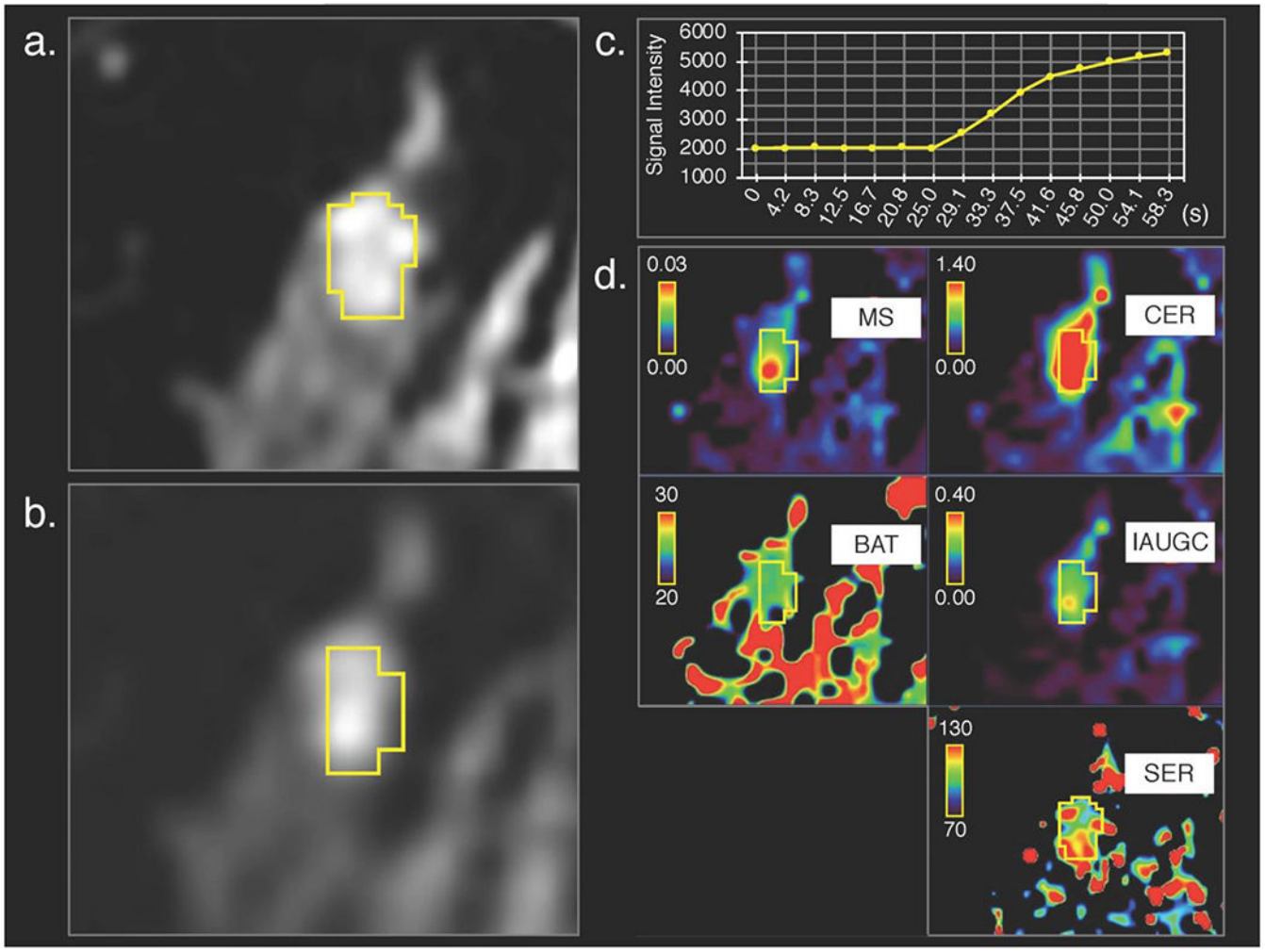

Figure 3:

Invasive lobular carcinoma in right breast of a 45-year-old woman, (a) 3D volumetric segmentation (yellow frame) was performed on the 1st phase of conventional dynamic contrast-enhanced magnetic resonance imaging (DCE-MRI) images and (b) cloned to all the other DCE-MRI phases; the 15th ultrafast DCE-MR image is shown as a representative, (c) Time-signal intensity (average of the whole lesion) curve of ultrafast DCE-MRI shows rapid increase of signal intensity and (d) parametric maps show difference between the lesion and surrounding tissue.

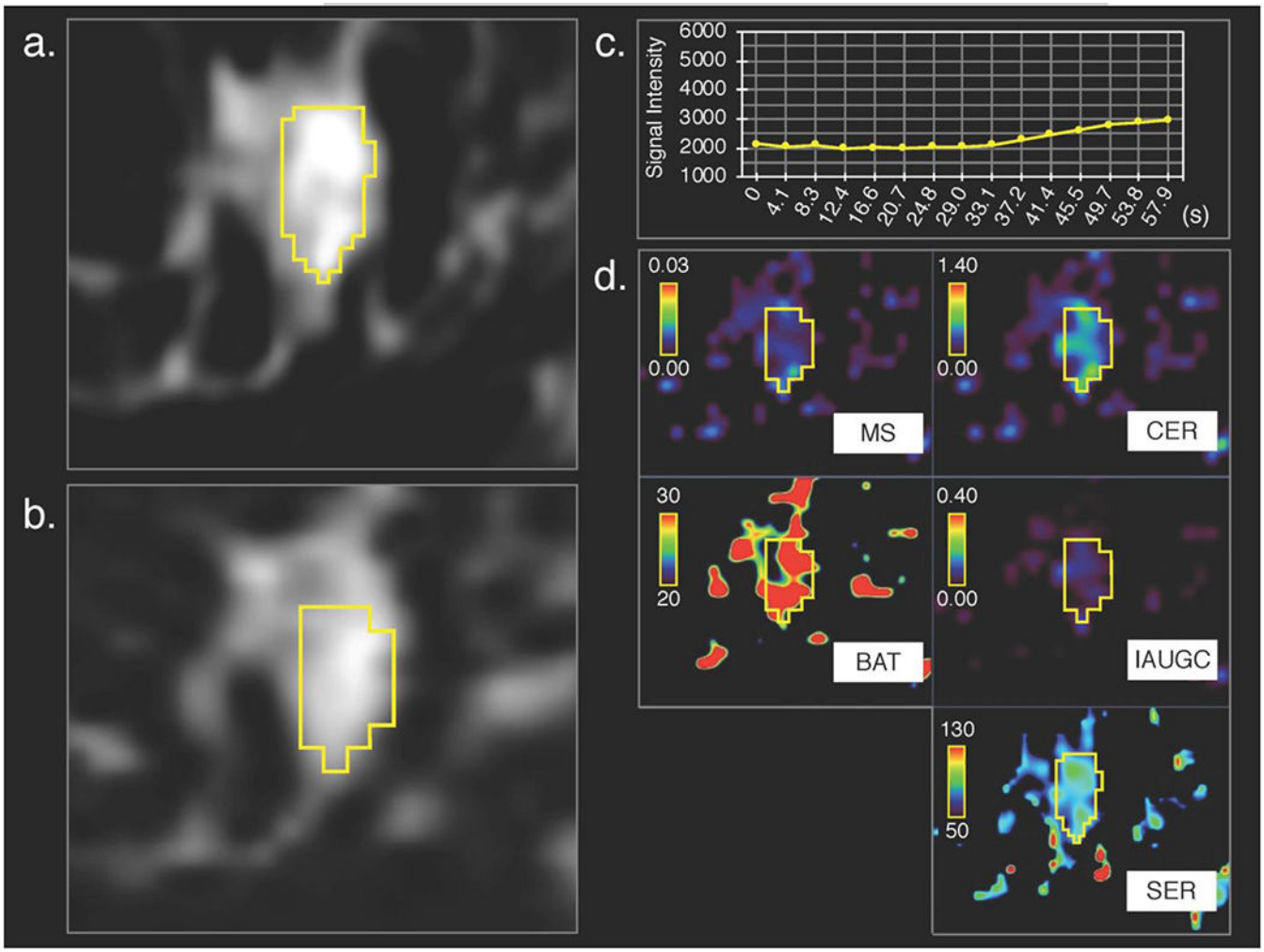

Figure 4:

Fibroadenoma in left breast of a 50-year-old woman, (a) 3D volumetric segmentation (yellow frame) was performed on the 1st phase of conventional dynamic contrast-enhanced magnetic resonance (DCE-MR) images, (b) cloned to all the other DCE-MRI phases; the 15th ultrafast DCE MR image is shown as a representative. Compared with invasive lobular carcinoma shown in Figure 3, (c) time–signal intensity (average of the whole lesion) curve of ultrafast DCE-MRI show slower increase of signal intensity and (d) parametric maps show less difference between the lesion and surrounding tissue.

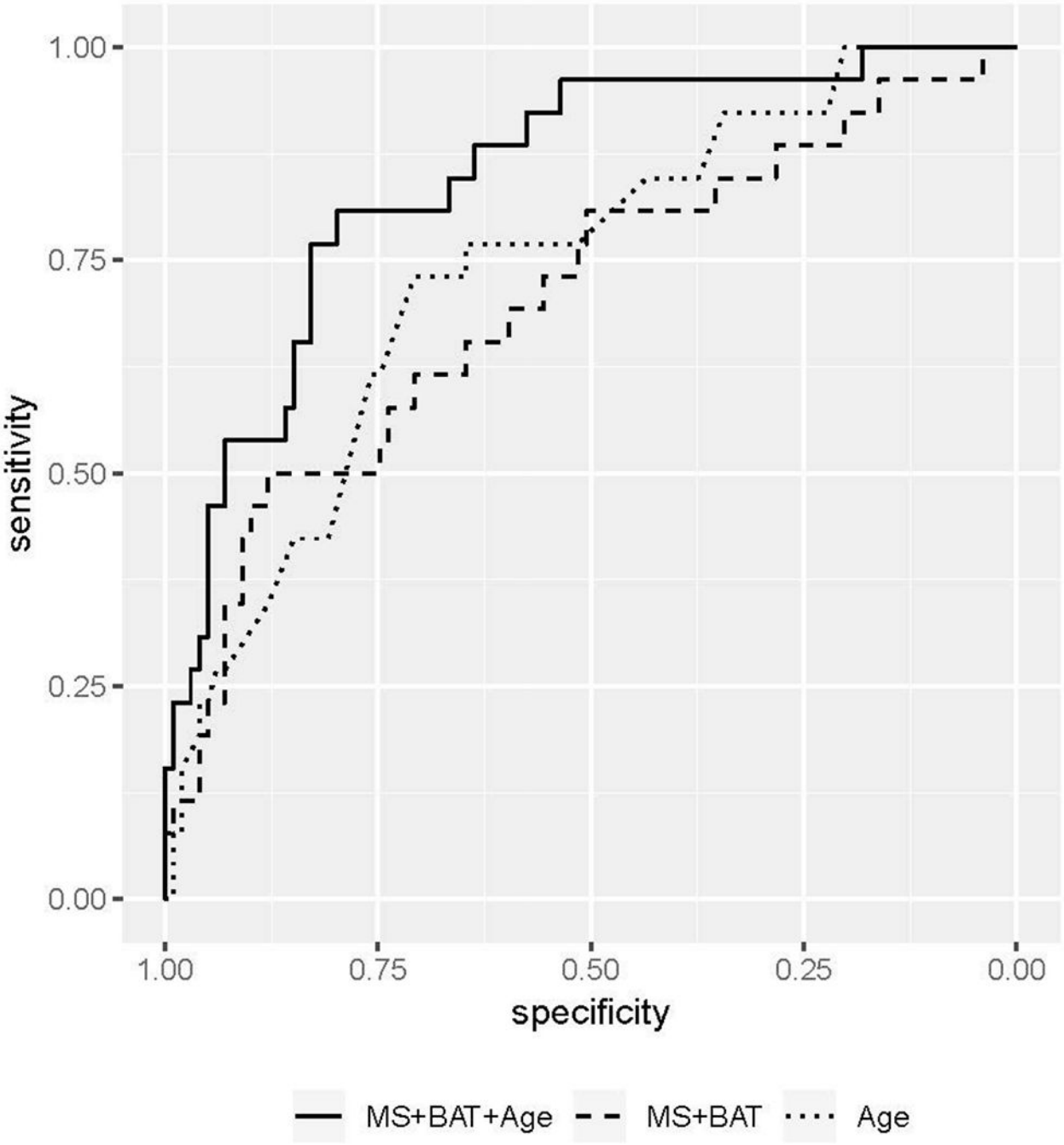

Figure 5:
ROC curves of the logistic regression models. The MS + BAT + age model, MS + BAT model, and age alone model showed an AUC of 0.846, 0.704, and 0.738 respectively. Maximum Youden index of the MS + BAT + age model was shown at a sensitivity of 81% and specificity of 80%.

Table 1

Lesion characteristics

	Subcentimeter C4&5 Group (n = 125)		Reference Group (n = 339)	
	Breast Carcinoma (n = 26)	**Benign Lesion (n = 99)**	**Breast Carcinoma (n = 225)**	**Benign Lesion (n = 114)**
Histopathology				
Invasive Ductal Carcinoma	7 (27%)		151 (67%)	
Invasive Lobular Carcinoma	9 (33%)		33 (15%)	
Mixed Invasive Ductal and Lobular Carcinoma	3 (12%)		11 (5%)	
Microinvasive Carcinoma	1 (4%)		7 (3%)	
DCIS	6 (23%)		23 (10%)	
High Risk Benign Lesion		11 (11%)		13 (11%)
Fibroadenoma		9 (9%)		13 (11%)
Papilloma		4 (4%)		4 (4%)
Others		75 (76%)		84 (74%)
Molecular Subtype *				
Luminal A/B Type (HR+,HER2−)	17 (89%)		129 (66%)	
Luminal-HER 2 Type (HR+, HER2+)	1 (5%)		32 (16%)	
HER2 Type (HR−, HER2+)	0 (0%)		12 (6%)	
Triple Negative Type (HR−, HER2−)	1 (5%)		22 (11%)	
LN Metastasis †				
Positive	2 (11%)		76 (41%)	
Negative	17 (89%)		110 (59%)	
Menopausal Status				
Pre-menopause	12 (46%)	71 (72%)	140 (62%)	83 (73%)
Post-menopause	14 (54%)	28 (28%)	85 (38%)	31 (27%)
Family History of Breast Cancer				
Positive	22 (85%)	65 (66%)	135 (60%)	75 (66%)
Negative	4 (15%)	34 (34%)	90 (40%)	39 (34%)
Family History of Ovarian Cancer				
Positive	2 (8%)	13 (13%)	15 (7%)	15 (13%)
Negative	24 (92%)	86 (87%)	210 (93%)	99 (87%)

Note.—Data represent the number of lesions and data in parentheses are percentages

* Invasive carcinomas of which molecular subtype were available

† Invasive carcinomas of which information of lymph node metastasis were available

Table 2

Comparison of kinetic parameters, size, and age between carcinomas and benign lesions

	Subcentimeter C4&5 Group (n = 125)			Reference Group (n = 339)		
	Breast Carcinoma (n = 26)	**Benign Lesion (n = 99)**	**P Value**	**Breast Carcinoma (n = 225)**	**Benign Lesion (n = 114)**	**P Value**
Ultrafast DCE MRI						
MS	0.0153 (0.0091–0.0253)	0.0101 (0.0072–0.0149)	0.0117 *	0.0386 (0.0182–0.0624)	0.0106 (0.0076–0.0147)	<0.0001 *
CER	1.033 (0.613–1.372)	0.912 (0.636–1.194)	0.3025	1.634 (1.093–2.206)	0.894 (0.636–1.181)	<0.0001 *
BAT	23.9 (20.9–27.3)	26.8 (23.7–29.5)	0.0102 *	22.4 (19.8–25.1)	26.8 (23.6–29.0)	<0.0001 *
IAUGC	0.170 (0.123–0.346)	0.146 (0.096–0.241)	0.1361	0.314(0.190–0.453)	0.142 (0.095–0.240)	<0.0001 *
Conventional DCE MRI						
SER	100.5 (89.6–124.7)	91.0 (80.9–100.7)	0.0046 *	107.7 (95.6–124.2)	88.4 (79.1–100.7)	<0.0001 *
Size						
Volume	0.122 (0.087–0.224)	0.113 (0.065–0.241)	0.5924	1.670 (0.435–6.510)	0.139 (0.073–0.321)	<0.0001 *
Diameter	0.75 (0.6–1.1)	0.8 (0.6–1.1)	0.8212	2.1 (1.3–3.4)	0.8 (0.6–1.3)	<0.0001 *
Age						
	55.0 (48.0–62.5)	45.0(40.0–53.0)	0.0002 *	49.0 (43.0–57.0)	45.0 (40.0–52.0)	0.0031 *

DCE-MRI, dynamic contrast-enhanced MRI; MS, maximum slope; CER, contrast enhancement ratio; BAT, bolus arrival time; IAUGC, initial area under the gadolinium contrast agent concentration time curve; SER, signal enhancement ratio.

* $p < 0.05$

Table 3

Comparison of BI-RADS morphological descriptors between carcinomas and benign lesions

	Subcentimeter C4&5 Group (n = 125)			Reference Group (n = 339)		
	Breast Carcinoma (n = 26)	**Benign Lesion (n = 99)**	**P Value**	**Breast Carcinoma (n = 225)**	**Benign Lesion (n = 114)**	**P Value**
Lesion Type			0.7342			< 0.0001 *
Mass	7 (27%)	26 (26%)		162 (72%)	29 (25%)	
Non Mass Enhancement	17 (65%)	58 (59%)		61 (27%)	70 (61%)	
Focus	2 (8%)	15 (15%)		2 (1%)	15 (13%)	
Mass						
Shape			0.7405			< 0.0001 *
Round	0 (0%)	1 (4%)		1 (1%)	1 (3%)	
Oval	2 (29%)	11 (42%)		6 (4%)	12 (41%)	
Irregular	5 (71%)	14 (54%)		155 (96%)	16 (55%)	
Margin			1			< 0.0001 *
Circumscribed	2 (29%)	8 (31%)		3 (2%)	8 (28%)	
Irregular	5 (71%)	17 (65%)		127 (78%)	20 (69%)	
Spiculated	0 (0%)	1 (4%)		32 (20%)	1 (3%)	
Internal Enhancement			1			0.0687
Homogeneous	0 (0%)	1 (4%)		1 (1%)	1 (1%)	
Heterogeneous	6 (86%)	20 (77%)		148 (91%)	23 (79%)	
Rim Enhancement	1 (14%)	5 (19%)		13 (8%)	5 (17%)	
Dark Internal Septations	0 (0%)	0 (0%)		0 (0%)	0 (0%)	
Non Mass Enhancement						
Distribution			0.0912			0.0007 *
Focal	13 (76%)	37 (64%)		32 (52%)	39 (56%)	
Linear	0 (0%)	13 (22%)		0 (0%)	13 (19%)	
Segmental	4 (24%)	6 (10%)		23 (38%)	14 (20%)	
Regional	0 (0%)	1 (2%)		3 (5%)	2 (3%)	
Multiple Regions	0 (0%)	1 (2%)		1 (2%)	1 (1%)	

	Subcentimeter C4&5 Group (n = 125)			Reference Group (n = 339)		
	Breast Carcinoma (n = 26)	Benign Lesion (n = 99)	P Value	Breast Carcinoma (n = 225)	Benign Lesion (n = 114)	P Value
Diffuse	0 (0%)	0 (0%)		2 (3%)	1 (1%)	
Internal Enhancement			0.6781			0.0052*
Homogeneous	0 (0%)	5 (9%)		1 (2%)	5 (7%)	
Heterogeneous	6 (32%)	18 (31%)		37 (61%)	26 (37%)	
Clumped	11 (65%)	35 (60%)		21 (34%)	39 (56%)	
Clustered Ring	0 (0%)	0 (0%)		2 (3%)	0 (0%)	

* p<0.05

Table 4

Univariate and multivariate logistic regression analysis in Subcentimeter C4&5 Group

Variables	Univariate Logistic Regression Analysis	Multivariate Logistic Regression Analysis			
	P Value	Beta Coefficient	Odds Ratio	95% Confidence Interval	P Value
MS	0.0078 *	34.907	1.44e+15	181, 5.89e+31	0.0208 *
BAT	0.0077 *	−0.208	0.812	0.694, 0.932	0.0023 *
SER	0.2610	NA	NA	NA	NA
Age	0.0003 *	0.123	1.131	1.070, 1.210	< 0.0001 *

MS, maximum slope; BAT, bolus arrival time; SER, signal enhancement ratio; NA, not available.

* $p<0.05$

Table 5

Diagnostic performances of the multivariate logistic regression model using maximum slope, bolus arrival time and age

Cut-off Point*	Sensitivity	Specificity	PPV	NPV	True Positive	True Negative	False Positive	False Negative
50%	35%	95%	64%	85%	9	94	5	17
40%	54%	93%	67%	88%	14	92	7	12
30%	62%	85%	52%	89%	16	84	15	10
23%†	81%	80%	51%	94%	21	79	20	5
20%	81%	78%	49%	94%	21	77	22	5
10%	92%	55%	35%	96%	24	54	45	2

PPV, positive predictive value; NPV, negative predictive value

Note.—Unless otherwise specified, data represent the number of lesions

*Cut-off point based on the probability for subcentimeter carcinoma calculated by the multivariate logistic regression model using maximum slope, bolus arrival time, and age.

†Cut-off point showing the maximum Youden index